ADVANCED ENERGY & SUSTAINABILITY RESEARCH
www.advenergysustres.com

Ring Defects Associated with Boron–Oxygen-Related Degradation in p-Type Silicon Heterojunction Solar Cells

Bruno Vicari Stefani, Moonyong Kim, Matthew Wright, Anastasia Soeriyadi, Ilya Nyapshaev, Konstantin Emtsev, and Brett Hallam*

Silicon heterojunction (SHJ) cell architectures, which have dominated silicon single-junction efficiency records for the past 10 years, are processed at relatively low temperatures, on the order of ≈250 °C. Recombination-active oxygen complexes in crystalline silicon, formed from interstitial oxygen (O_i), typically require temperatures higher than this to form. Therefore, it is typically assumed that SHJ cells are immune to such defects. This contrasts with the high-temperature passivated emitter and rear cell (PERC) and tunneling oxide passivating contact (TOPCon) architectures, which can suffer from oxygen precipitates that are recombination active and difficult to predict. Herein, ring-like defects are observed in boron-doped p-type SHJ solar cells, which leads to a degradation of open-circuit voltage. It is shown that the spatial variation of this recombination activity is related to the boron–oxygen defect, the variation of which is likely due to the radial O_i distribution. Although boron-doped p-type wafers are no longer the industry standard, the defect engineering of wafers for SHJ production, using high-temperature processing, is gaining significant interest. Such wafers can have an increased susceptibility to ring-like defects. Therefore, spatially inhomogeneous defects causing recombination may become increasingly relevant for SHJ cells.

1. Introduction

The silicon heterojunction (SHJ) technology has enabled world-record power conversion efficiencies in single-junction silicon solar cells.[1] When combined with an interdigitated back contact (IBC) contacting scheme, SHJ solar cells achieved a conversion efficiency of 27.30%.[2] In a traditional front and back contact scheme, SHJ solar cells achieved a peak conversion efficiency of 26.81% on an n-type Czchoralski-grown crystalline silicon (Cz-Si) wafer.[3]

Laboratory and industrial SHJ solar cells are traditionally based on n-type wafers. The three main reasons for using n-type wafers are 1) lower susceptibility to recombination caused by metallic impurities, 2) the susceptibility of p-type boron-doped wafers to boron–oxygen-related light (in fact, carrier)-induced degradation, and 3) challenges with surface passivation of p-type wafers.[4,5] Recent progress in defect-engineering of SHJ solar cells combined, with the availability of high-lifetime gallium-doped (Ga-doped) Cz-Si wafers, resulted in high-efficiency[6,7] and stable[6,8] p-type SHJ solar cells, including a record conversion efficiency of 26.56%.[7] This record p-type efficiency is only ≈0.2%$_{abs}$ lower than its n-type counterpart (both cells using a front and back contacting scheme). Work from Chang et al. indicates (assuming a wafer premium of 8% for n-type wafers) that replacing n- by p-type wafers in SHJ manufacturing may be cost effective if the efficiency gap between p-type and n-type can reach 0.4%$_{abs}$.[9] The recent high-efficiency results for p-type indicate there may be an economic incentive to investigate the use of this cheaper wafer type in manufacturing. When trap-assisted recombination in the silicon bulk is excluded, theoretical modeling indicates a higher conversion efficiency limit for p-type compared to n-type SHJ solar cells.[7] Thus, the economic incentive to replace n- by p-type wafers could become more favorable as approaches to reduce trap-assisted recombination in the silicon bulk are further improved.

Apart from traditional rigid modules, there has been recent progress in the development of thin (and flexible) SHJ solar cells, with demonstrated conversion efficiencies exceeding 25% for n-type[10] and p-type[7] wafers. Thin and flexible lightweight SHJ modules are of particular interest for space photovoltaics.[11] In such application, p-type wafers show greater stability (under electron radiation) than their n-type counterparts.[12] Therefore, progress in defect engineering of SHJ solar cells can also contribute to the development of thin solar cells for space applications.

B. Vicari Stefani, M. Kim, B. Hallam
School of Photovoltaics and Renewable Energy Engineering
UNSW
Sydney, NSW 2052, Australia
E-mail: moonyong.kim@unsw.edu.au

M. Wright, A. Soeriyadi
Department of Materials
University of Oxford
Oxford OX1 3PH, UK

I. Nyapshaev, K. Emtsev
R&D Center of Thin Film Technologies in Energetics
St. Petersburg 194064, Russia

The ORCID identification number(s) for the author(s) of this article can be found under https://doi.org/10.1002/aesr.202400255.

DOI: 10.1002/aesr.202400255

Table 1. Current–Voltage characteristics of the p-type boron-doped Czchoralski-grown SHJ solar cells.

Number of cells	η [%]	J_{SC} [mA cm^{-2}]	V_{OC} [mV]	FF [%]
22	20.8 ± 0.4	39.2 ± 0.1	723.2 ± 6.3	73.6 ± 1.0
Best-performing cell				
–	21.5	38.8	726.5	75.6

The Cz-Si wafers used in solar cell manufacturing are susceptible to oxygen-related recombination-active defects, such as thermal donors.[13,14] These defects are related to the relatively high concentrations of oxygen introduced during Cz-Si ingot growth.[15–17] Oxygen-related defects in Cz-Si wafers can appear as rings, which can be seen via photoluminescence (PL) imaging.[15] The radial nonuniformity of these defects is related to the low segregation coefficient of oxygen in silicon, which is considerably smaller than unity, resulting in higher impurity concentration in the center of Cz-Si wafers.[18] The radial gradient in impurity concentration is impacted by ingot growth conditions.[19]

Oxygen-related defects can limit the η of solar cells fabricated with such wafers. Haunschild et al. observed conversion efficiency losses of $4\%_{abs}$ (initial efficiency $> 18\%$) due to the presence of ring defects.[20] Thermal donors are thought to be formed via the aggregation of silicon and interstitial oxygen atoms.[13,21] Their formation can occur at a wide temperature range (with peak formation rates at ≈470 °C) and it relates to the wafer's thermal history.[22] Annealing the wafers at temperatures >600 °C can annihilate thermal donors.[23] Thus, homojunction designs, such as the passivated emitter and rear cell (PERC) and tunnel oxide passivating contact or polysilicon on oxide (TOPCon/POLO), are not significantly impacted by thermal donors. This is related to the high-temperature processing routes used to manufacture PERC and TOPCon cells, where p-n junction formation and metallization occur at temperatures well above 600 °C. SHJ solar cells, on the other hand, are traditionally manufactured at temperatures <250 °C.[4] The low-temperature regime used for cell fabrication prevents the potential formation of thermal donors during cell fabrication. However, it also prevents the annihilation of thermal donors generated during crystal growth. In this article, we report the occurrence of ring-like defects in SHJ solar cells fabricated with p-type boron-doped (B-doped) wafers for the first time. We investigate the defect behavior under illumination and the impact of an advanced hydrogenation process on passivating the defect.

2. Results and Discussion

2.1. Boron–Oxygen-Related Degradation

We fabricated SHJ solar cells with p-type B-doped Cz-Si wafers. These wafers did not undergo prefabrication defect engineering processes. The solar cells exhibited an average conversion efficiency of 20.8% and an average open-circuit voltage of 723 mV. **Table 1** displays the cells' current–voltage characteristics. PL imaging of the solar cells unraveled the presence of ring-like defects (see **Figure 1**a).

Ring defects typically represent nonuniform concentrations of oxygen impurity in the wafers. The susceptibility of B-doped Cz-Si wafers to the boron–oxygen (BO) defect can exacerbate the negative impact of these ring defects on solar cell performance. The BO defect concentration is known to increase quadratically with the concentration of interstitial oxygen and substitutional boron.[24] Consequently, spatial variations in the concentration of boron and oxygen can result in spatial variations of BO defects.[25,26] Thus, we next investigate the potential correlation between the observed ring and BO defects.

We first subjected a p-type B-doped SHJ solar cell to a light-soaking (LS) process to fully form BO defects. During LS, the cells were kept at 25 °C for 48 h while the entire cell area was illuminated using an LED light source with an intensity equivalent to 0.02 suns. This illumination intensity was selected because it allows the generation of BO defects[27,28] while ensuring that $\Delta n \ll N_A$ and minimizing the impact of other potential carrier-induced effects. The ring defects were found to be exacerbated after LS (see Figure 1b). PL imaging highlighted a

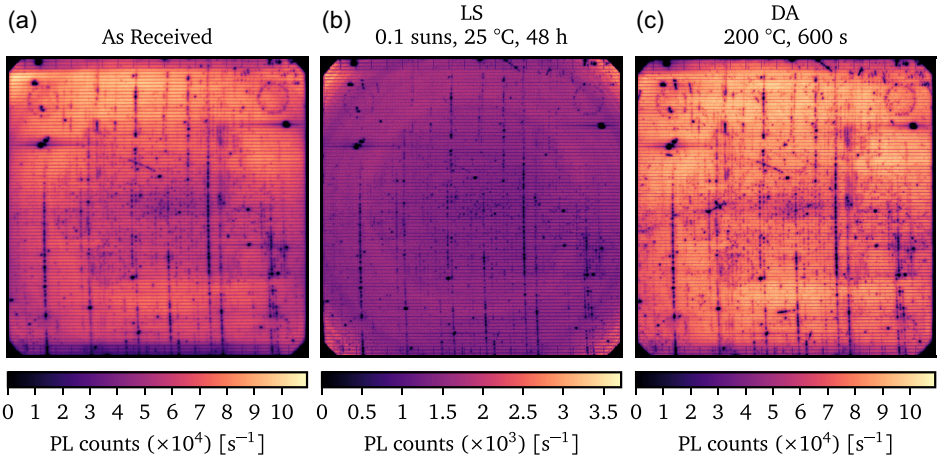

Figure 1. PL images of SHJ solar cell fabricated with p-type boron-doped wafers a) before any additional processing, b) after light soaking (LS), and c) after dark annealing (DA).

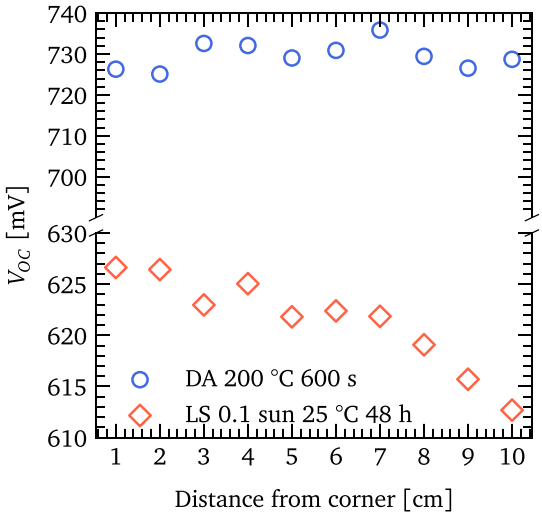

Figure 2. Open-circuit voltage (V_{OC}) as a function of distance from the solar cell's corner after light soaking (LS) for boron–oxygen (BO) defect formation (red diamonds) and after dark annealing (DA) for BO defect annihilation (blue circles).

gradient in PL counts, where the wafer corners exhibited >2 times greater counts than the center region. We performed local Suns-V_{OC} measurements using a point probe as a function of distance from the cell corner. The Suns-V_{OC} measurements allow us to quantify the changes in wafer quality in terms of injection-dependent V_{OC}.

We annealed the same p-type B-doped SHJ solar cell in the dark to anneal all BO defects. This allows for the assessment of the limiting lifetime (thus PL response and V_{OC}) when all BO defects are recombination inactive. The sample was annealed for 600 s at 200 °C.[29] We recorded PL images (see Figure 1c) and Suns-V_{OC} measurements using the same procedure. The V_{OC} values as a function of distance from the cell corner are shown in **Figure 2**.

The spatial distribution of V_{OC} agrees with the trend observed via PL imaging. V_{OC} is higher (≈626 mV) at the cell edges than in the center (≈613 mV) when BO defects are fully formed (i.e., after LS). Yet, the V_{OC} distribution is much more uniform when BO defects are fully annealed (after DA). We calculated the relative boron–oxygen defect concentration (N^*_{BO}) as a function of the distance from the cell corner using Equation (1) and the carrier lifetime at a minority carrier density (Δn) of 1.4×10^{14} cm^{-3}, where $\tau_{degraded}$ is the lifetime after LS, and $\tau_{annealed}$ is the lifetime after DA. **Figure 3**a illustrates where we performed local Suns-V_{OC} measurements as a function of distance from the cell corner and Figure 3b presents the corresponding N^*_{BO} values.

$$N^*_{BO} = \frac{1}{\tau_{BO}} = \frac{1}{\tau_{degraded}} - \frac{1}{\tau_{annealed}} \quad (1)$$

We observed that N^*_{BO} varies spatially across the wafer. The cell exhibits an N^*_{BO} of ≈0.08 µs^{-1} close to the edges and a N^*_{BO} ≈0.13µs^{-1} on its center, corresponding to a >60% increase in N^*_{BO} This result agrees with the findings from Lim et al.[26] In their study, the authors found N^*_{BO} to depend on the distance from the wafers' edge—albeit a variation of one order of magnitude was reported. Lim et al. attributed the N^*_{BO} spatial variation to a spatial variation in interstitial oxygen concentration, given they observed the boron dopant concentration to be much more uniform.

The root cause of spatial variations in defect concentration cannot be confirmed solely based on the PL and current (or suns) and voltage measurements performed. Yet, the observation of ring-like defects indicates that the spatial distribution of defects might be caused by spatial variations in interstitial oxygen concentration. This hypothesis is supported by the observation of increased or decreased recombination activity upon BO defect formation or annihilation, respectively.

We modeled the V_{OC} as a function of defect concentration to verify whether the observed changes in V_{OC} between the DA and LS states could also be explained by a uniform distribution of N*$_{BO}$ combined with a nonuniform background recombination

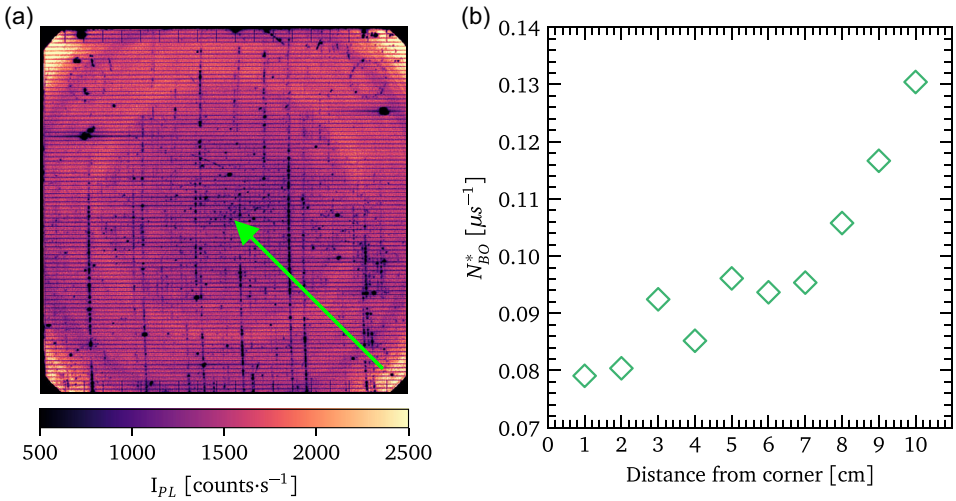

Figure 3. a) PL images of a p-type B-doped SHJ solar cell illustrating the region when Suns-V_{OC} measurements were taken (green arrow). b) Relative boron–oxygen defect concentration N^*_{BO} as a function of the distance from the solar cell's corner.

associated with the ring-like defects. We calculated the injection-dependent effective lifetime (τ_{eff}) before and after BO-LID based on Equation (2), where τ_{BO} is the lifetime associated with the BO defect, $\tau_{SRH,background}$ is the background SRH lifetime, $\tau_{surface}$ is the surface lifetime, and $\tau_{intrinsic}$ is the intrinsic lifetime.

$$\frac{1}{\tau_{eff}} = \frac{1}{\tau_{BO}} + \frac{1}{\tau_{SRH,background}} + \frac{1}{\tau_{surface}} + \frac{1}{\tau_{intrinsic}} \quad (2)$$

We then used the resulting minority carrier density as a function of defect concentration to calculate the expected 1 sun V_{OC} based on Equation (3), where k is the Boltzmann constant, T is the temperature, q is the elementary charge, N_A is the bulk dopant concentration, and Δn is minority carrier density at 1 sun equivalent illumination.

$$V_{OC} = \frac{kT}{q}\ln\left(\frac{\Delta n(N_A + \Delta n)}{n_i^2}\right) \quad (3)$$

We fixed the intrinsic and surface-related lifetimes while varying both the k-value and concentration of a background SRH defect [$SRH_{background}$]. The V_{OC} as a function of defect capture cross-sectional ratios (k) and defect concentration is shown in **Figure 4**, where the solid line represents the V_{OC} before LID. We then added the BO lifetime component ([SRH_{BO}]) to represent the lifetime after LID. The concentration of [SRH_{BO}] was equal to the lower bound of [$SRH_{background}$]. The V_{OC} after LID is represented by the dashed lines in Figure 4. The results in Figure 4 indicate that a large (>30 mV) V_{OC} gap before LID is required to yield small (≈1 mV) variations in the V_{OC} after LID.

However, when we fix [$SRH_{background}$] concentration and vary [SRH_{BO}], the model accurately describes the nonuniform V_{OC} variation after LID. The modeled (lines) and measured (markers) V_{OC} as a function of [SRH_{BO}] before and after LID are displayed in **Figure 5**. These results support the hypothesis that the nonuniform defect concentration observed via PL imaging is predominantly caused by a nonuniform distribution of BO defects. However, we note that variations in the background recombination (either present before LID or formed during LS despite the mild conditions) can also contribute to a lower degree.

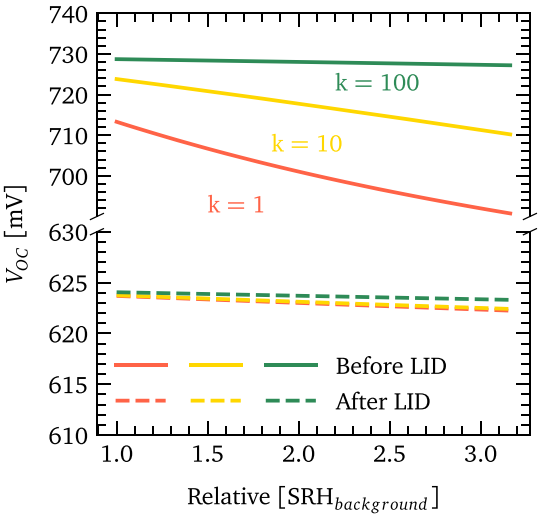

Figure 4. Modeled open-circuit voltage (V_{OC}) as a function of relative [$SRH_{background}$] with capture cross-sectional ratios (k) of 1 (red lines), 10 (yellow lines), and 100 (green lines) before (solid lines) and after (dashed lines) boron–oxygen light-induced degradation (BO-LID).

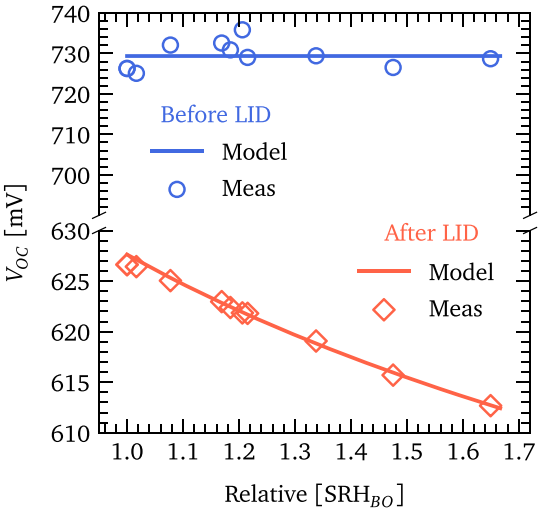

Figure 5. Measured (markers) and modeled (lines) open-circuit voltage (V_{OC}) as a function of relative [SRH_{BO}] before (blue) and after (red) boron–oxygen light-induced degradation (BO-LID).

2.2. Advanced Hydrogenation

Illuminated annealing treatments are now widely used to improve cell conversion efficiency in SHJ manufacturing.[30] These treatments were shown to improve surface passivation[31] and charge carrier transport[32,33] in SHJ solar cells. In our previous work, we found that advanced hydrogenation processes (AHP) commonly used for defect passivation in homojunction p-type solar cells can also be used for illuminated annealing of SHJ solar cells, regardless of wafer type and polarity.[34]

AHP treatments can stabilize BO defects in p-type boron-doped SHJ solar cells. The stable V_{OC} after treatment is dependent on the processing conditions and initial BO defect concentration.[5] Thus, one could expect a nonuniform stable V_{OC} after AHP for a cell that exhibits a nonuniform spatial distribution of N^*_{BO}. To test this hypothesis, we applied an AHP treatment in two small (52 × 52 mm) samples sourced from two different areas of a p-type SHJ solar cell. We first LS these samples to fully form BO defects. This was followed by an AHP treatment and a second LS to form any residual BO defects not stabilized during AHP. **Figure 6** shows the PL images of samples cut from the a) corner and d) center of a p-type SHJ solar cell after the initial LS. We note that the PL intensity (I_{PL}) is higher closer to the edge when BO defects are fully formed. The AHP treatment increased the overall I_{PL} of both samples to the same level (depicted in Figure 6b,e), indicating a more uniform distribution of I_{PL} ($\propto V_{OC}$) when BO defects are recombination inactive (either in the annealed or stabilized states). After a subsequent LS, we observed a reduction in the I_{PL} of both samples (depicted in

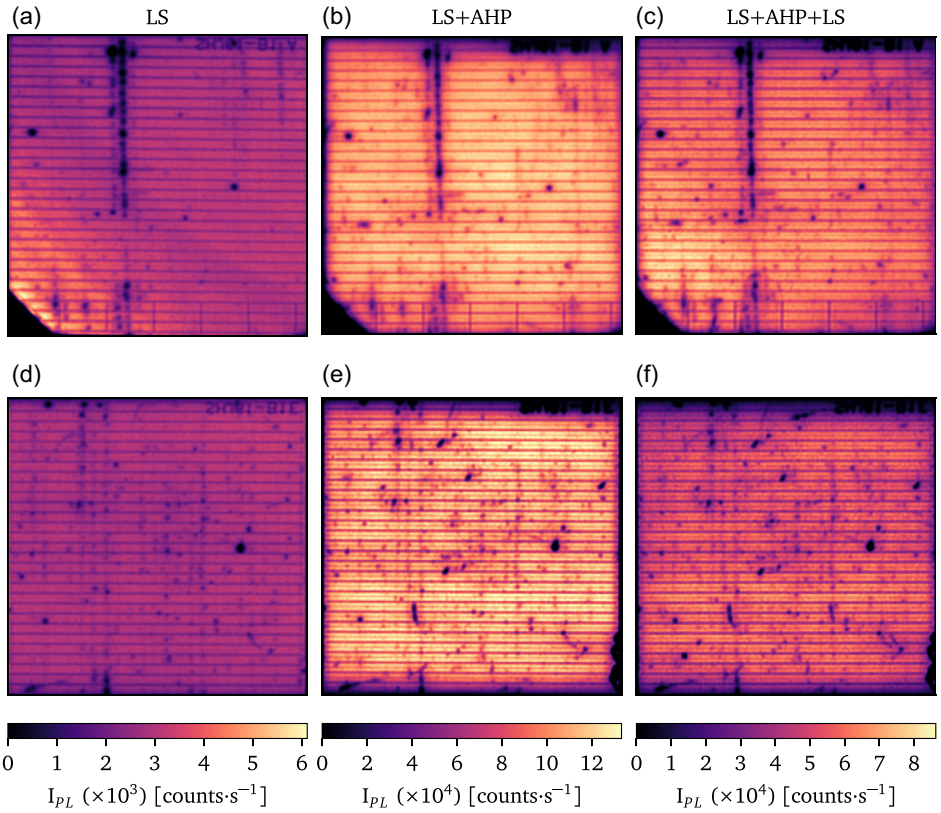

Figure 6. PL images of samples sourced from the a–c) corner and d–f) center of a p-type boron-doped SHJ solar cell. (a,d) Taken after light soaking (LS) (48 h, 25 °C, 0.02 suns), (b,e) taken after an advanced hydrogenation process (AHP), and (c,f) taken after subsequent stability testing via LS (48 h, 25 °C, 0.02 suns).

Figure 6c,f), which is expected due to the formation of residual BO defects not stabilized during AHP.

Yet, the relative reduction in I_{PL} was different for the two samples. The center sample displayed an I_{PL} reduction of ≈45–60%. In contrast, the corner sample displayed a much lower reduction in I_{PL} reaching ≈20% in the outermost area. These changes are depicted in **Figure 7**. We cannot quantify the N^*_{BO} based solely on the PL images as they were registered at a fixed generation rate, which results in changes in the injection-level across the wafer. However, these observations

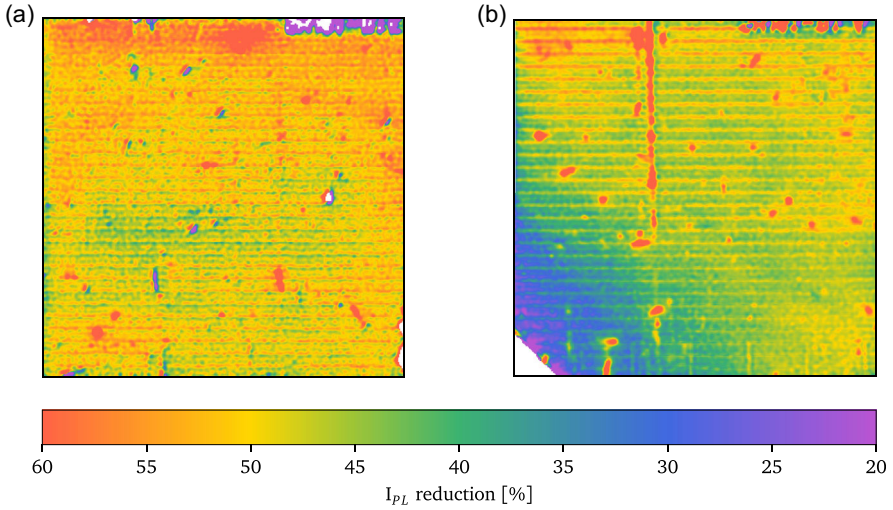

Figure 7. Reduction in the intensity PL counts (I_{PL}) after stability testing via light soaking on advanced hydrogenation-treated samples sourced from the a) center and b) corner of a *p*-type boron-doped SHJ solar cell.

provide evidence that the stabilization of BO defects in p-type SHJ solar cells can vary spatially, possibly due to nonuniform distribution of N^*_{BO}. The results discussed in this section highlight the high defect concentration present in the wafers and reinforces the importance of limiting the initial N^*_{BO} via wafer-level defect engineering treatments (such as gettering[35,36]) to facilitate subsequent BO defect stabilization via AHP.

3. Conclusion

Herein, we fabricated SHJ solar cells using commercial-grade p-type Cz-Si wafers. These cells presented ring-like defects, which limited cell performance. We identified a radial distribution of BO defect activity in the cells through a combination of PL imaging and local Suns-V_{OC} measurements. We observed nonuniform magnitude of BO-LID across the solar cell area, where areas of high degradation corresponded to ring-affected areas. The correlation between the BO defect and ring defects observed via PL imaging is thought to be caused by a radial nonuniformity of interstitial oxygen concentration. Further work is required to quantify the radial distribution of impurities in the wafers. These observations demonstrate the susceptibility of low-temperature solar cell fabrication routes to ring defects introduced during crystal growth. Finally, these results highlight the importance of high temperature (>600 °C) prefabrication defect-engineering processes for SHJ solar cells. Such processes have been widely adopted in SHJ manufacturing,[30] can benefit both p- and n-type SHJ solar cells,[34] and were used in the fabrication of the 26.56% record p-type SHJ solar cell.[7] Further work is required to verify whether prefabrication defect-engineering processes can mitigate ring defects in SHJ solar cells fabricated with commercial-grade wafers susceptible to such defects.

4. Experimental Section

Bifacial SHJ solar cells were fabricated in an industrial pilot line by R&D Center TFTE LLC using 156.75 × 156.75 mm B-doped silicon wafers with a resistivity of 0.8 Ω cm. These wafers were commonly used in the fabrication of PERC solar cells and were acquired from SAS Sunrise. The wafers underwent KOH-based saw-damage etch and anisotropic texturing, resulting in a thickness of ≈165 µm. This was followed by a cleaning step to remove organic and metallic contaminants. A stack of intrinsic and B-doped hydrogenated amorphous silicon layers was deposited on the wafers' rear. A stack of intrinsic and phosphorus-doped hydrogenated amorphous silicon layers was then deposited on the wafers' front. Both depositions were performed using a plasma-enhanced chemical vapor deposition tool. A physical vapor deposition tool was used to deposit indium tin oxide layers on both sides of the wafers. The front and rear busbarless metallization was screen printed using low-temperature silver paste followed by a curing step. *J*–*V* measurements were performed at R&D Center TFTE LLC directly after cell fabrication using a GridTOUCH contacting unit for busbarless solar cells and a PASAN SpotLIGHT HighCap tester under standard testing conditions. PL images of finished SHJ solar cells were taken with a BTImaging LIS-R3 tool at 1 sun illumination intensity. We performed localized V_{OC} measurements using a point probe in a WCT-120 lifetime tester Suns-V_{OC} stage (Sinton Instruments).

Acknowledgements

This work was supported by the Australian Government through the Australian Centre for Advanced Photovoltaics (ACAP) and the Australian Renewable Energy Agency (ARENA) (2017/RND005). The views expressed herein are not necessarily the views of the Australian Government, and the Australian Government does not accept responsibility for any information or advice contained herein. This work was funded by UK Research and Innovation (UKRI) under the UK government's Horizon Europe funding guarantee [101109417]. M.K. acknowledges the support of ACAP for his postdoctoral fellowship. The authors would like to thank Dr. Dmitriy Andronikov and Dr. Sergey Abolmasov for the fruitful scientific discussions and assistance with cell processing in this work.

Conflict of Interest

The authors declare no conflict of interest.

Author Contributions

Bruno Vicari Stefani: Conceptualization (lead); Data curation (lead); Formal analysis (lead); Investigation (lead); Methodology (lead); Software (lead); Validation (lead); Visualization (lead); Writing—original draft (lead). **Moonyong Kim**: Conceptualization (supporting); Investigation (supporting); Methodology (supporting); Supervision (supporting); Writing—review & editing (supporting). **Matthew Wright**: Investigation (supporting); Methodology (supporting); Supervision (supporting); Writing—original draft (supporting); Writing—review & editing (supporting). **Anastasia Soeriyadi**: Investigation (supporting); Supervision (supporting). **Ilya Nyapshaev**: Investigation (supporting); Resources (supporting); Writing—review & editing (supporting). **Konstantin Emtsev**: Investigation (supporting); Resources (supporting). **Brett Hallam**: Funding acquisition (lead); Investigation (supporting); Methodology (supporting); Project administration (lead); Resources (lead); Supervision (lead); Validation (supporting); Writing—review & editing (supporting).

Data Availability Statement

The data that support the findings of this study are available from the corresponding author upon reasonable request.

Keywords

boron, heterojunctions, oxygen, p-types, silicon

Received: August 19, 2024
Revised: October 23, 2024
Published online: November 20, 2024

[1] M. A. Green, E. D. Dunlop, M. Yoshita, N. Kopidakis, K. Bothe, G. Siefer, X. Hao, *Prog. Photovoltaics* **2024**, *32*, 3.
[2] Long. Green Energy Technology Co, *LONGi News* **2024**.
[3] H. Lin, M. Yang, X. Ru, G. Wang, S. Yin, F. Peng, C. Hong, M. Qu, J. Lu, L. Fang, C. Han, P. Procel, O. Isabella, P. Gao, Z. Li, X. Xu, *Nat. Energy* **2023**, *8*, 789.
[4] S. De Wolf, A. Descoeudres, Z. C. Holman, C. Ballif, *Green* **2012**, *2*, 7.
[5] B. Vicari Stefani, M. Wright, A. Soeriyadi, D. Chen, M. Kim, B. Wright, D. Andronikov, I. Nyapshaev, S. Abolmasov, G. Wilson, B. Hallam, *Sol. RRL* **2022**, *6*, 2200449.
[6] A. Danel, N. Chaugier, J. Veirman, R. Varache, M. Albaric, E. Pihan, *Prog. Photovoltaics Res. Appl.* **2023**, *31*, 1235.
[7] X. Ru, M. Yang, S. Yin, Y. Wang, C. Hong, F. Peng, Y. Yuan, C. Sun, C. Xue, M. Qu, J. Wang, J. Lu, L. Fang, H. Deng, T. Xie, S. F. Liu, Z. Li, X. Xu, *Joule* **2024**, *8*, 1092.

[8] B. Vicari Stefani, M. Kim, M. Wright, A. Soeriyadi, D. Andronikov, I. Nyapshaev, S. Abolmasov, K. Emtsev, A. Abramov, B. Hallam, *Sol. RRL* **2021**, *5*, 2100406.
[9] N. L. Chang, M. Wright, R. Egan, B. Hallam, *Cell Rep. Phys. Sci.* **2020**, *1*, 100069.
[10] Y. Li, X. Ru, M. Yang, Y. Zheng, S. Yin, C. Hong, F. Peng, M. Qu, C. Xue, J. Lu, L. Fang, C. Su, D. Chen, J. Xu, C. Yan, Z. Li, X. Xu, Z. Shao, *Nature* **2024**, *626*, 105.
[11] R. Cariou, A. Danel, N. Enjalbert, F. Jay, S. Dubois, *IEEE J. Photovoltaics* **2024**, *14*, 41.
[12] K. D. Smith, H. K. Gummel, J. D. Bode, D. B. Cuttriss, R. J. Nielsen, W. Rosenzweig, *Bell Syst. Tech. J.* **1963**, *42*, 1765.
[13] M. Chatelain, M. Albaric, D. Pelletier, J. Veirman, E. Letty, *Sol. Energy Mater. Sol. Cells* **2021**, *219*, 110785.
[14] J. Veirman, R. Varache, M. Albaric, A. Danel, B. Guo, N. Fu, Y. C. Wang, *Sol. Energy Mater. Sol. Cells* **2021**, *228*, 111128.
[15] T. Niewelt, S. Lim, J. Holtkamp, J. Schön, W. Warta, D. Macdonald, M. C. Schubert, *Sol. Energy Mater. Sol. Cells* **2014**, *131*, 117.
[16] B. Martel, J. Veirman, M. Cascant, N. Enjalbert, M. Tomassini, R. Peyronnet, J. Stadler, E. Fayard, S. Dubois, G. Raymond, X. Brun, P. Bonnard, in *2015 IEEE 42nd Photovoltaic Specialist Conf. (PVSC)*, IEEE, New Orleans, LA **2015**, pp. 1–3.
[17] T. Mehl, I. Burud, E. Letty, E. Olsen, *Energy Procedia* **2017**, *124*, 107.
[18] W. Lin, M. Stavola, *J. Electrochem. Soc.* **1985**, *132*, 1412.
[19] W. Lin, *Semiconductors and Semimetals*, Elsevier, London **1994**, pp. 9–52.
[20] J. Haunschild, I. E. Reis, J. Geilker, S. Rein, *Phys. Status Solidi RRL* **2011**, *5*, 199.
[21] F. Jay, J. Veirman, N. Najid, D. Muñoz, S. Dubois, A. Jouini, *Energy Procedia* **2014**, *55*, 533.
[22] V. V. Voronkov, G. I. Voronkova, A. V. Batunina, V. N. Golovina, R. J. Falster, M. Cornara, N. B. Tiurina, A. S. Guliaeva, *Solid State Phenomena* **2009**, *156*, 115.
[23] H. J. Stein, S. K. Hahn, S. C. Shatas, *J. Appl. Phys.* **1986**, *59*, 3495.
[24] T. Niewelt, J. Schon, W. Warta, S. W. Glunz, M. C. Schubert, *IEEE J. Photovoltaics* **2017**, *7*, 383.
[25] D. Walter, B. Lim, K. Bothe, R. Falster, V. Voronkov, J. Schmidt, in *Proc. 27th European Photovoltaic Solar Energy Conf. Exhibition*, Frankfurt **2012**.
[26] S. Y. Lim, F. E. Rougieux, D. Macdonald, *Appl. Phys. Lett.* **2013**, *103*, 092105.
[27] H. Hashigami, Y. Itakura, T. Saitoh, *J. Appl. Phys.* **2003**, *93*, 4240.
[28] J. Schmidt, K. Bothe, *Phys. Rev. B* **2004**, *69*, 024107.
[29] M. Kim, M. Abbott, N. Nampalli, S. Wenham, B. Stefani, B. Hallam, *J. Appl. Phys.* **2017**, *121*, 053106.
[30] S. K. Chunduri, M. Schmela, *Heterojunction Solar Technology Report 2023, Taiyang News* **2023**.
[31] J. Veirman, A. J. K. Leoga, L. Basset, W. Favre, O. Bonino, A. L. Priol, N. Rochat, D. Rouchon, in *AIP Conf. Proc.*, Vol. *2487*, Hamelin, Germany **2022**, p. 020017.
[32] W. Liu, J. Shi, L. Zhang, A. Han, S. Huang, X. Li, J. Peng, Y. Yang, Y. Gao, J. Yu, K. Jiang, X. Yang, Z. Li, W. Zhao, J. Du, X. Song, J. Yin, J. Wang, Y. Yu, Q. Shi, Z. Ma, H. Zhang, J. Ling, L. Xu, J. Kang, F. Xu, J. Liu, H. Liu, Y. Xie, F. Meng, S. De Wolf, F. Laquai, Z. Di, Z. Liu, *Nat. Energy* **2022**, *7*, 427.
[33] M. Wright, A. H. Soeriyadi, M. Kim, B. Wright, B. V. Stefani, D. Andronikov, I. Nyapshaev, S. Abolmasov, A. Abramov, R. S. Bonilla, B. Hallam, *Sol. Energy Mater. Sol. Cells* **2022**, *248*, 112039.
[34] M. Wright, B. Vicari Stefani, A. Soeriyadi, R. Basnet, C. Sun, W. Weigand, Z. Yu, Z. Holman, D. Macdonald, B. J. Hallam, *Phys. Status Solidi RRL* **2021**, *15*, 2100170.
[35] K. Bothe, R. Sinton, J. Schmidt, *Prog. Photovoltaics* **2005**, *13*, 287.
[36] N. Nampalli, H. Li, M. Kim, B. Vicari Stefani, S. Wenham, B. Hallam, M. Abbott, *Sol. Energy Mater. Sol. Cells* **2017**, *173*, 12.